iScience, Volume *26*

Supplemental information

Enhanced cell viscosity: A new phenotype associated with lamin A/C alterations

Cécile Jebane, Alice-Anaïs Varlet, Marc Karnat, Lucero M. Hernandez- Cedillo, Amélie Lecchi, Frédéric Bedu, Camille Desgrouas, Corinne Vigouroux, Marie-Christine Vantyghem, Annie Viallat, Jean-François Rupprecht, Emmanuèle Helfer, and Catherine Badens

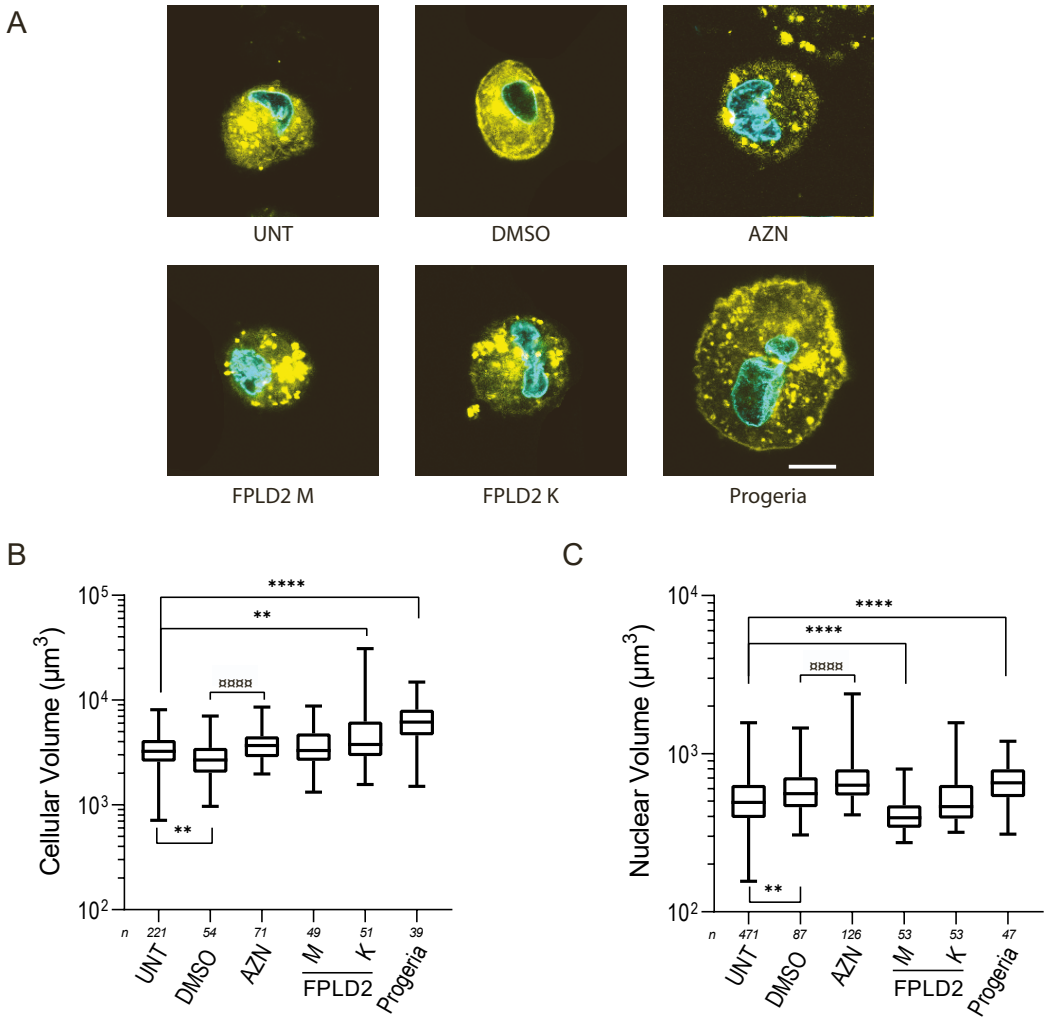

D

Cell	Cellular Volume (μm^3)		Nuclear Volume (μm^3)	
	Median	95% CI	Median	95% CI
UNT	3254	3068-3457	491	469-511
DMSO	2678	2294-3022	558	511-598
AZN	3677	3192-4205	633	591-686
FPLD2 M	3310	2986-3731	393	350-432
FPLD2 K	3775	3490-4495	462	413-578
Progeria	6171	4976-7635	654	568-737

Fig. S1. Cellular and nuclear volumes of control and altered lamin A/C cells. Related to Figure 2. Volumes were quantified to design the microfluidic devices. UNT: untreated control cells; DMSO: control cells incubated with DMSO for 48 h; AZN: control cells treated with Atazanavir (in DMSO) for 48 h; M,K: cells from two patients with FLPD2 carrying the lamin A/C R482W mutation; Progeria: cells from a patient with HGPS carrying the lamin A/C G608G mutation. Adhered cells were labelled for plasma membrane (with CellBrite) and nuclei (with Hoechst) before detachment and resuspension in culture medium. Cellular and nuclear volumes were computed from confocal imaging. A) Typical confocal planes of cells (in yellow) and nuclei (in cyan). Scale bar: 10 µm. B-C) Boxplot representations of the cellular (A) and nuclear (B) volumes, with median values, 25% and 75% percentiles, and min/max values as whiskers. Significant differences: FPLD2, Progeria and DMSO cells *vs* UNT cells, *; AZN *vs* DMSO cells, ¤. D) Table recapitulating median values of the volumes and 95% Confidence Intervals (CIs). Number of experiments: N $\geq$ 2; number of analyzed cells: *n*.

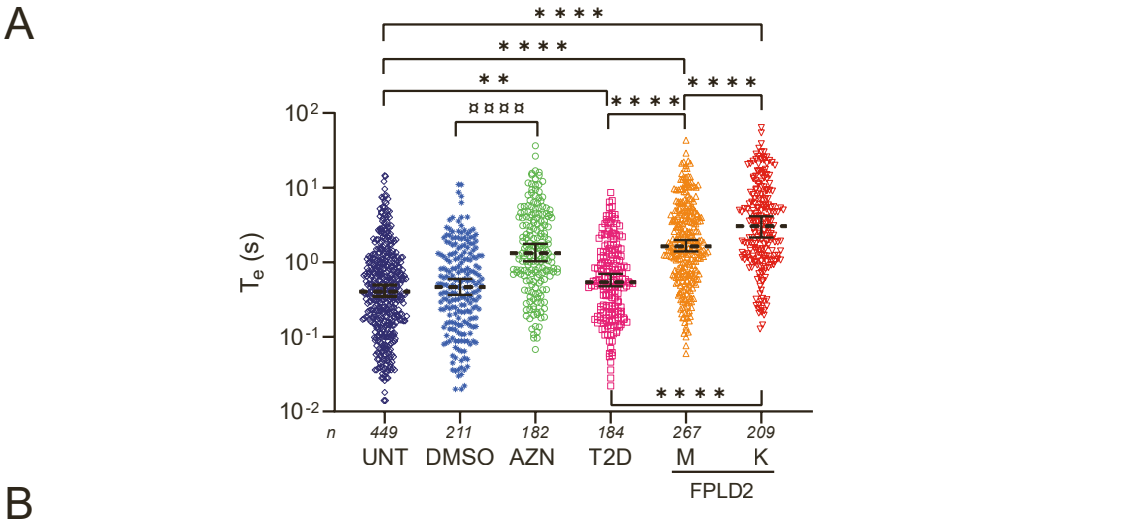

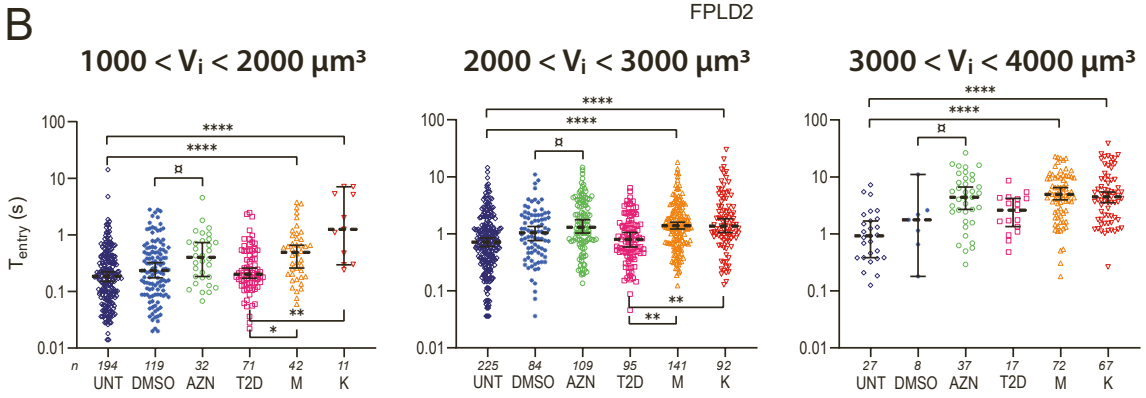

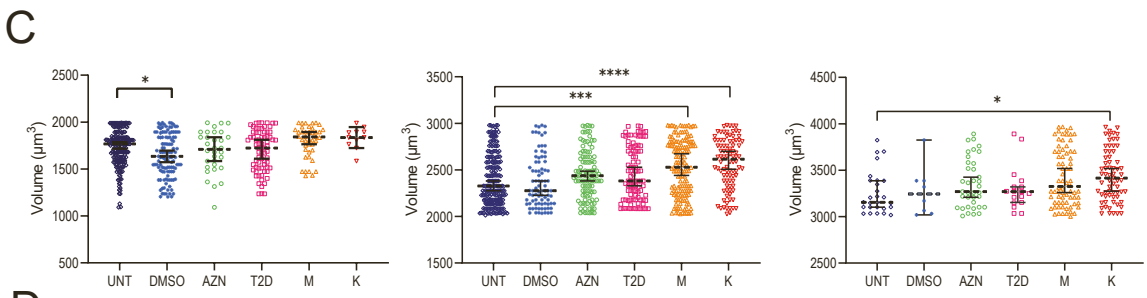

D

	Median entry time Te [95% CI] (s)			Median volume [95% CI] (µm³)		
	1000 < 2000 µm³	2000 < 3000 µm³	3000 < 4000 µm³	1000 < 2000 µm³	2000 < 3000 µm³	3000 < 4000 µm³
UNT	0.186 [0.152-0.222]	0.714 [0.600-0.848]	0.928 [0.384-1.688]	1768 [1716-1787]	2328 [2276-2382]	3155 [3102-3387]
DMSO	0.234 [0.174-0.323]	1.041 [0.764-1.344]	1.773 [0.180-11.09]	1635 [1573-1696]	2276 [2228-2382]	3245 [3019-3825]
AZN	0.402 [0.184-0.732]	1.304 [1.032-1.768]	4.412 [2.688-6.648]	1710 [1584-1838]	2437 [2382-2486]	3270 [3208-3425]
T2D	0.202 [0.172-0.260]	0.798 [0.588-1.052]	2.610 [1.340-4.198]	1724 [1610-1811]	2382 [2329-2529]	3270 [3152-3320]
FPLD2 M	0.490 [0.260-0.656]	1.392 [1.220-1.592]	4.930 [3.964-6.520]	1842 [1764-1895]	2529 [2441-2673]	3325 [3259-3519]
FPLD2 K	1.254 [0.296-7.092]	1.362 [1.060-1.844]	4.472 [3.544-5.428]	1836 [1724-1947]	2615 [2506-2699]	3415 [3275-3519]

Fig. S2. Entry time in constrictions T_e is larger in altered lamin A/C cells independently of cell size. Related to Figure 3. Cell types as in Fig. 3: UNT: untreated control cells; DMSO: control cells incubated with DMSO for 48 h; AZN: control cells treated with Atazanavir for 48 h; T2D: cells from the diabetic patient; M,K: cells from the patients with FPLD2. A) Dotplot representation of T_e, independently of cell size. The non-Gaussian distributions are plotted in log scale; median values and 95% CIs are indicated. The plots correspond to the bar plots in Fig. 3A and illustrate the number of analysed cells. B) Same plots as in (A), with cells sorted into three size populations (volume bin: 1000 µm^3). The cellular volumes were computed from the images of the cells before they enter the microfluidic constrictions. Both types of cells with lamin A/C alterations, FPLD2 and AZN, display larger T_e compared to their respective controls, whatever the volume range. C) Dotplot representation of cell volumes per volume bin. Within a bin, the median volumes differ by at most 12% between cell types. D) Table recapitulating median values and 95% CIs of entry times and cell volumes per volume bin. Significant differences: FPLD2 *vs* T2D *vs* UNT cells, *; AZN *vs* DMSO cells, ¤. Number of experiments: N $\geq$ 3; number of analyzed cells: *n*.

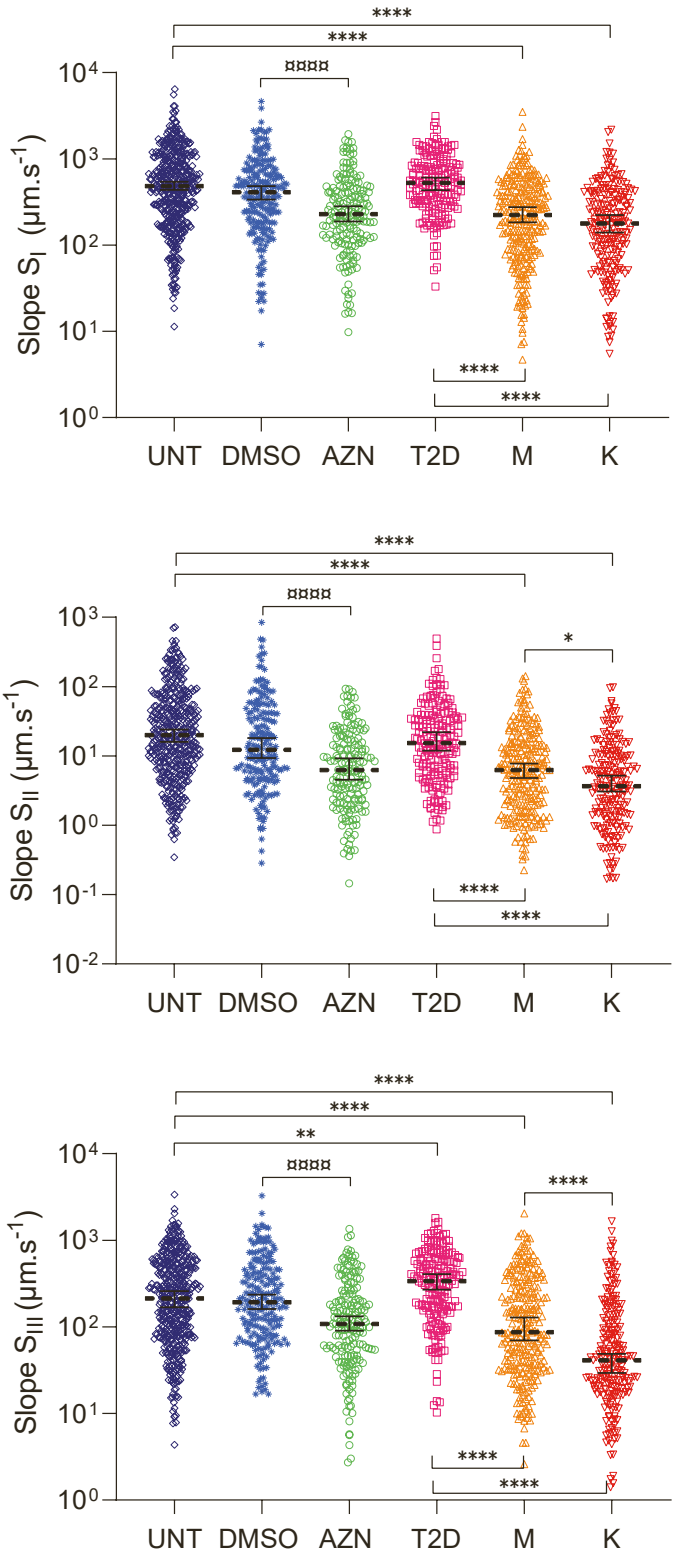

Fig. S3. The linear slopes $S_I - S_{III}$ of the three regimes in the temporal curve of the tongue length $\ell(t)$ are changed by the cell condition, consistently with the entry time T_e. Related to Figure 3A. Significant differences: FPLD2 *vs* T2D *vs* UNT cells, *; AZN *vs* DMSO cells, ¤. Number of experiments: N $\geq$ 3; number of analyzed cells: *n* > 150.

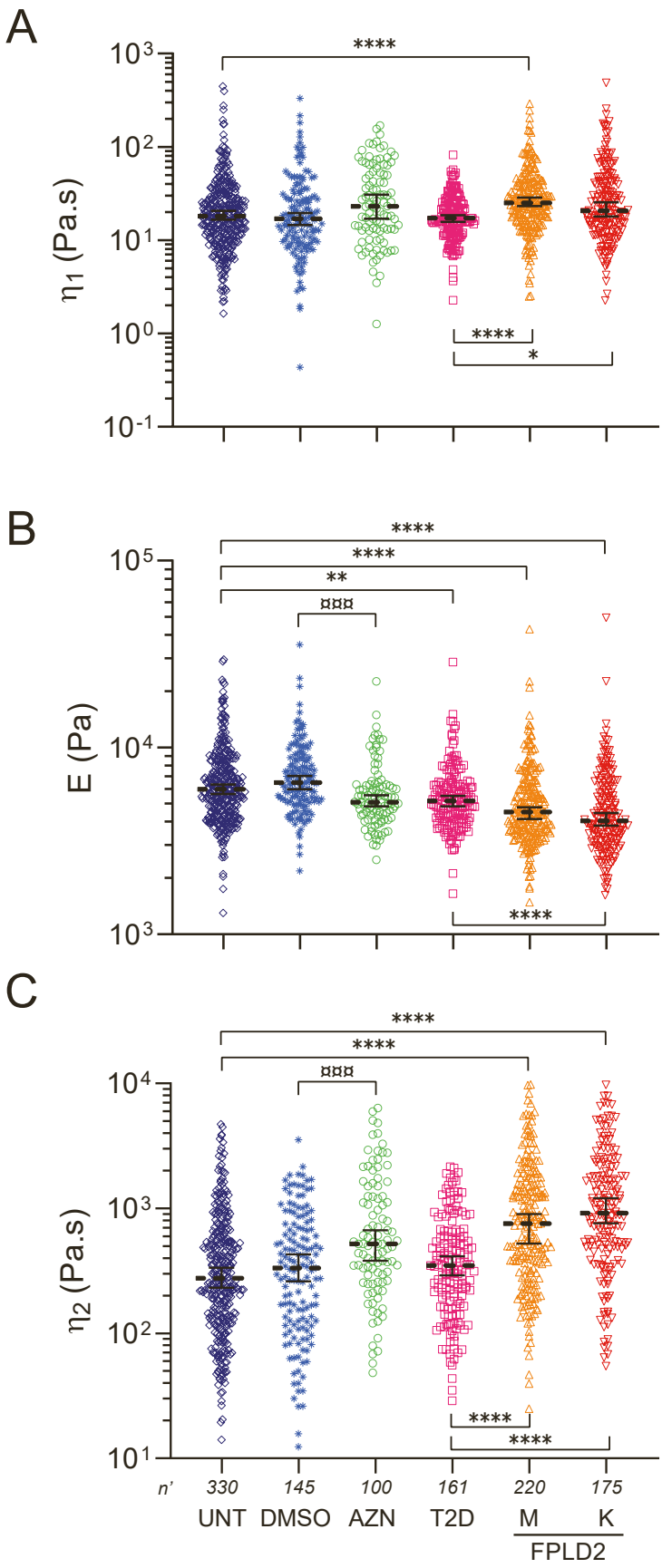

Fig. S4. Dotplot representations of cell viscoelastic parameters extracted with the rheological model. Related to Figure 3. The plots correspond to the bar plots in Fig. 3D-F and illustrate the number of analyzed cells. A) Short-time viscosity η_1. B) Elastic modulus E. C) Long-time viscosity η_2. Significant differences: FPLD2 *vs* T2D *vs* UNT cells, *; AZN *vs* DMSO cells, ¤. Number of experiments : N $\geq$ 3 ; number of fitted curves: *n'*.

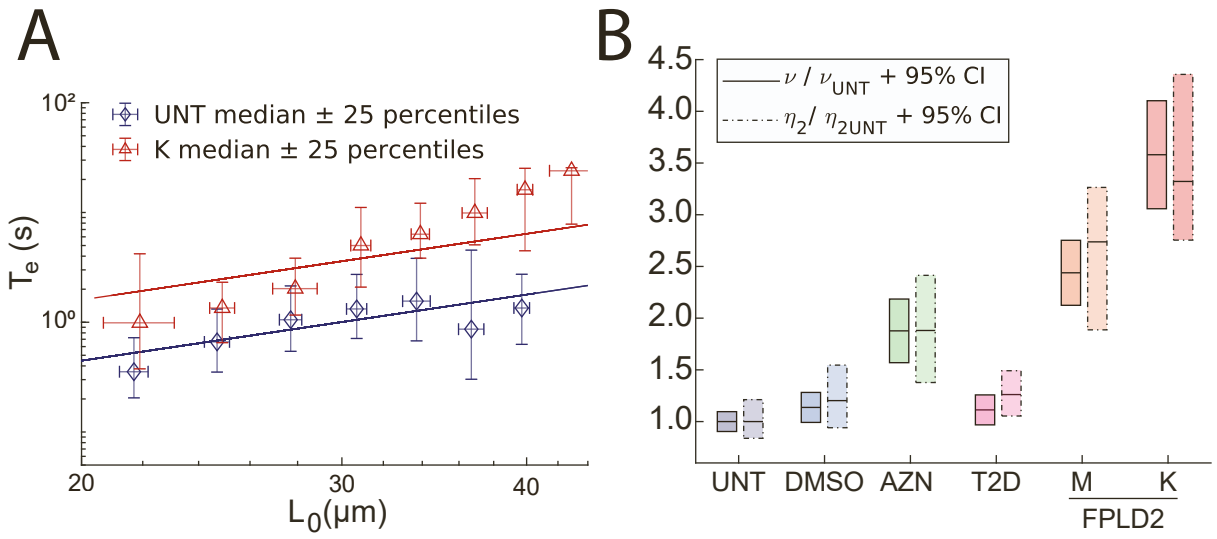

Fig. S5. Alteration of long time viscosity is detected by a simple relationship between entry time and cell initial length. Related to Figure 3F. A) Dependence of the entry time T_e with the cell initial length L_0 for UNT and K cells. Data are plotted in log-log scale and fitted with the scaling law $T_e \sim \nu L_0^2$. Cells with T_e < 0.3 s were not considered. Data were binned using a length bin set to 3 µm. Medians values are displayed with 25% percentiles. B) Boxplots of the constant ν extracted from the scaling law fit (solid line) and of long-time viscosity η_2 (dashed line), normalized to the values obtained for UNT cells (median values $\pm$ 95% CIs).

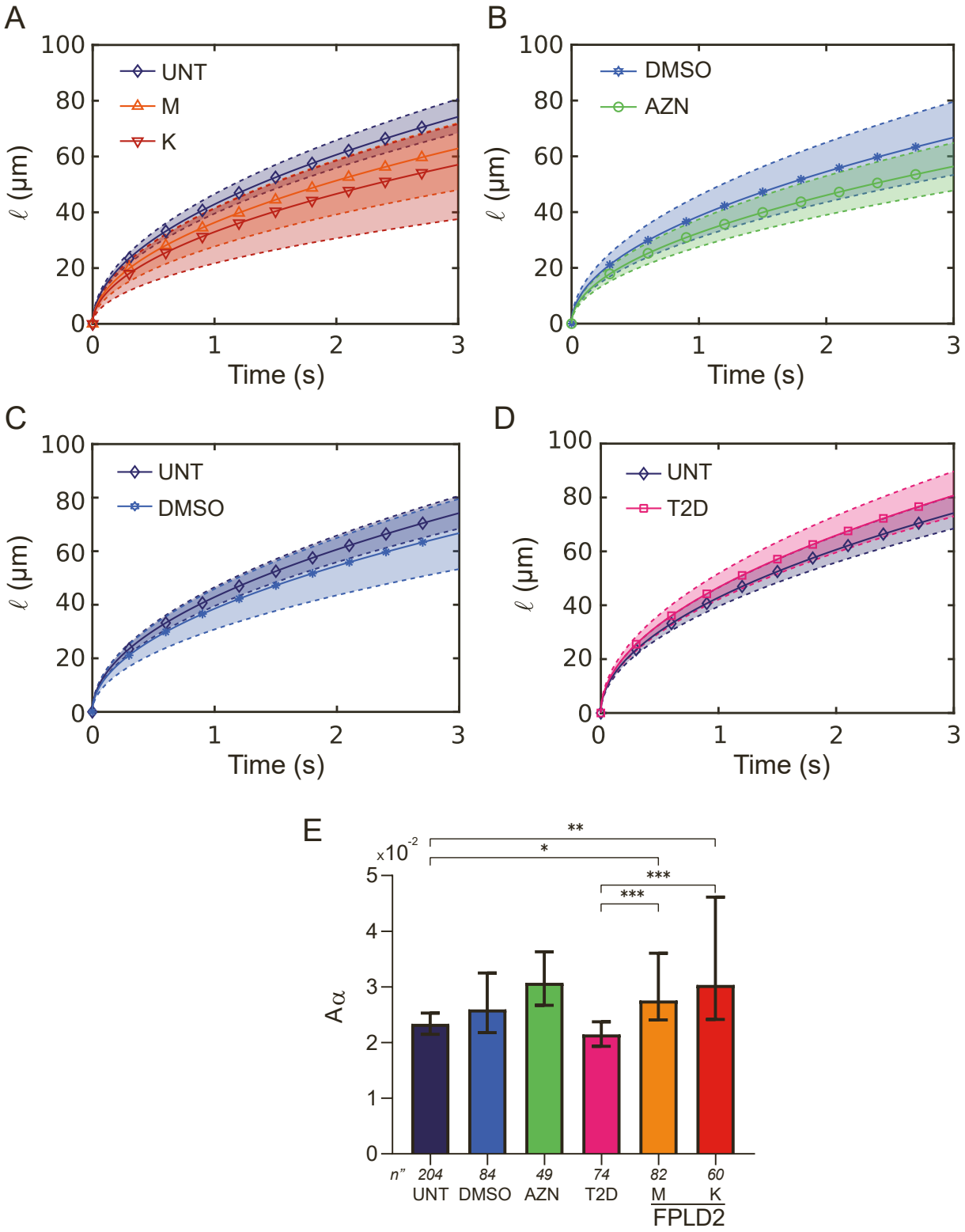

Fig. S6. Tongue length fits using a power law. Related to Figures 3F and S7. A-D) Power law fits $\ell = \ell_0 + t^{0.5}/A_\alpha$ for UNT *vs* M and K cells (A), DMSO *vs* AZN cells (B), UNT *vs* DMSO cells (C), and UNT *vs* L cells (D). Solid curves and symbols indicate the median fits plotted with the median values of the parameters, dashed upper and lower curves delineate the 95% CIs. E) Comparison of A_α values extracted from the power law fits for the different cell types (medians $\pm$ 95% CIs). Significant differences: FPLD2 *vs* T2D *vs* UNT cells, *; AZN *vs* DMSO cells, ¤. Number of experiments: N $\geq$ 3; number of fitted curves: *n"*.

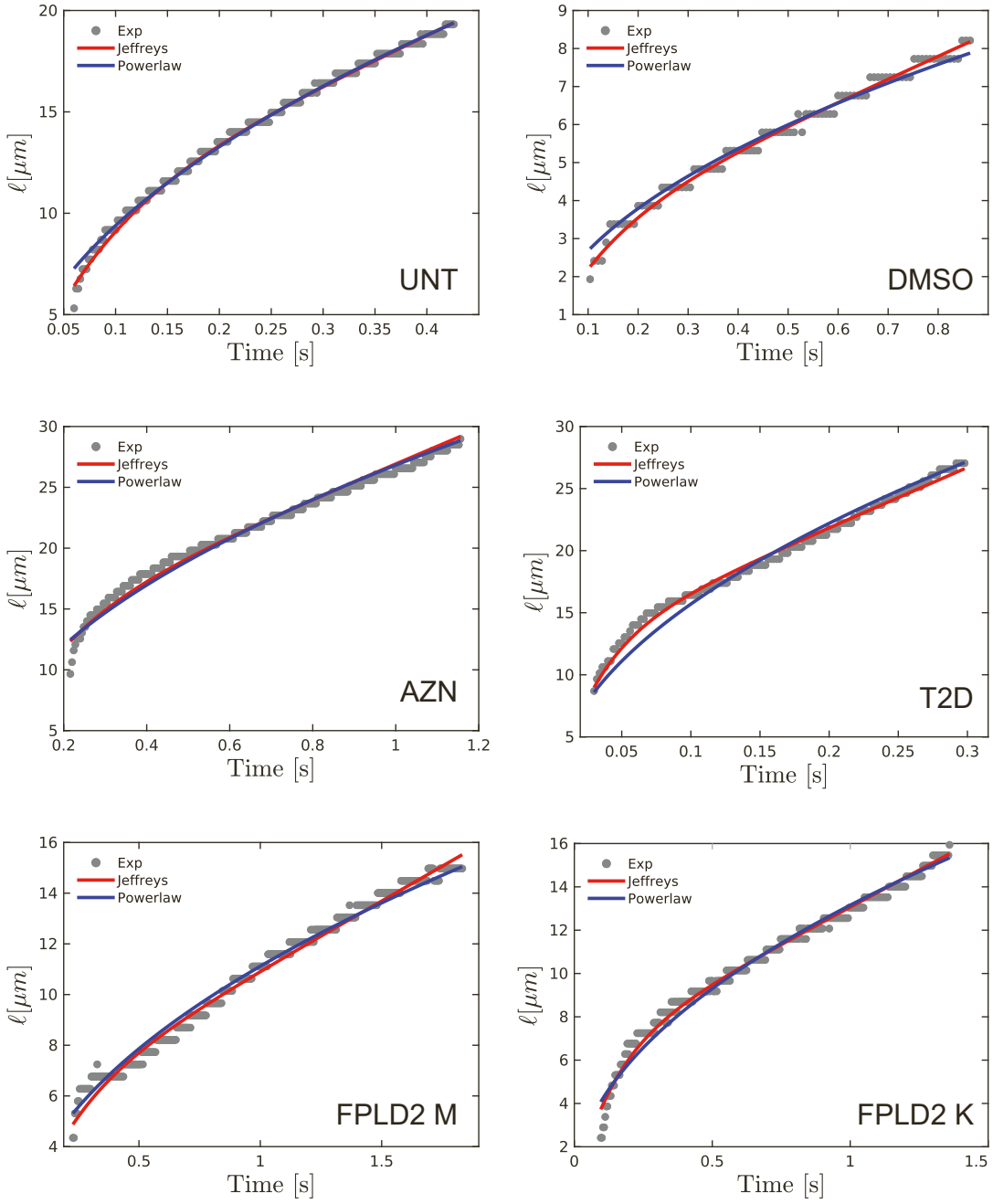

Fig. S7. Typical cell tongue elongation curves fitted with Jeffreys and power law models. Related to Figures 3 and S6. Cells as in Fig. 3.

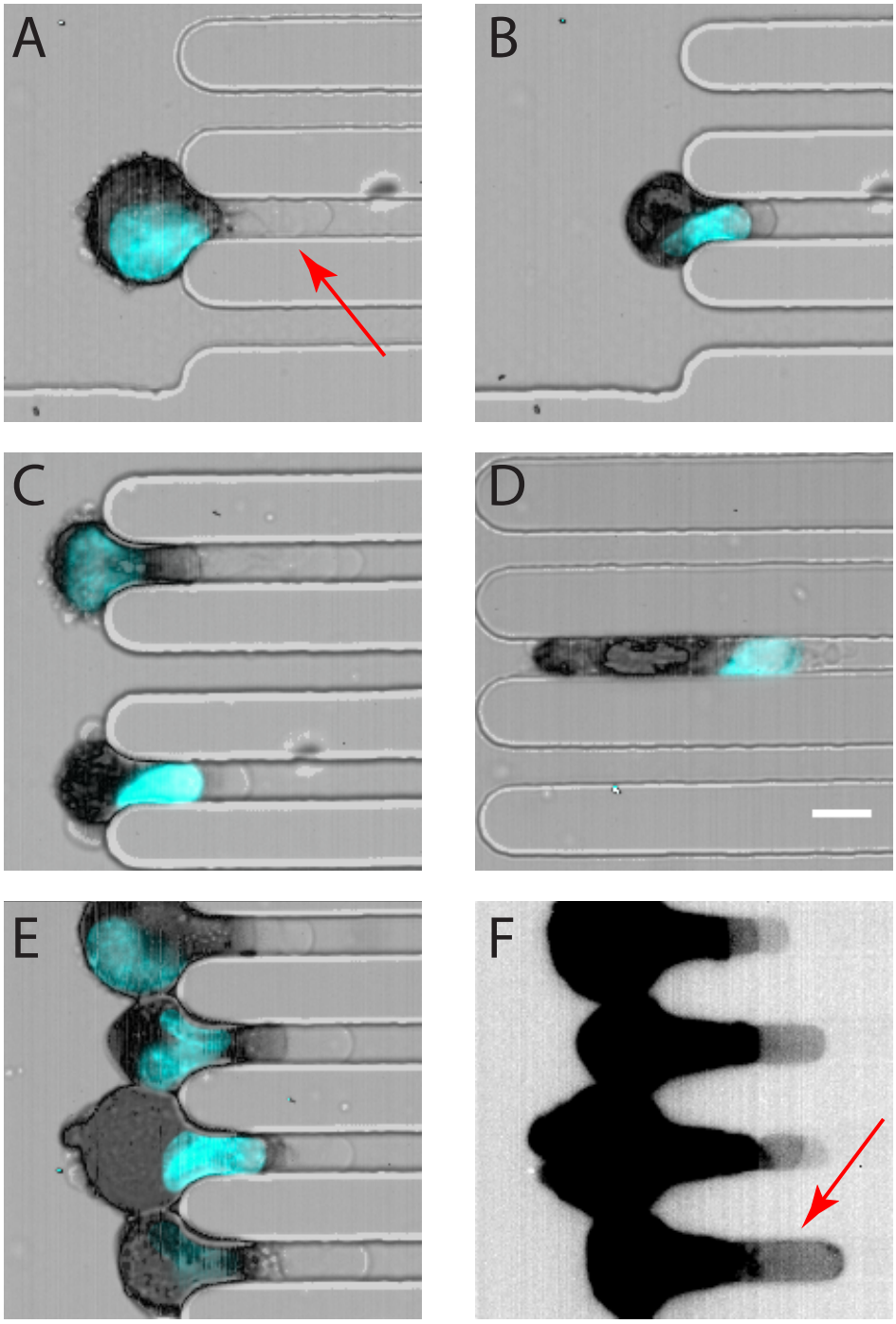

Fig. S8. The cell forms a bleb at the front that precedes the actin cortex and the nucleus during deformation in the constriction. Related to Figure 3D and Table 1. The cell membrane, actin and nucleus are imaged at different timepoints during entry in constriction. A) The cell comes into contact with the constriction and a bleb immediately enters (phase I). B) The bleb moves forward, the actin cortex and the nucleus slowly deform (phase II). C) The nucleus has completely entered the constriction and the rear of the cell deforms (bottom cell), the bleb is still present at the front (phase III). D) The cell is fully deformed and transits through the constriction, with the bleb at the front followed by actin, nucleus and cell rear (phase IV). E-F) Saturating the image highlights the transparent front bleb, with the actin in black. Cell membrane is imaged in brightfield; nucleus and F-actin are imaged in epifluorescence, via Hoechst (blue) and SPY-actin 555 (black) labelling, respectively. Red arrows indicate some blebs. Scale bar = 10 μm.

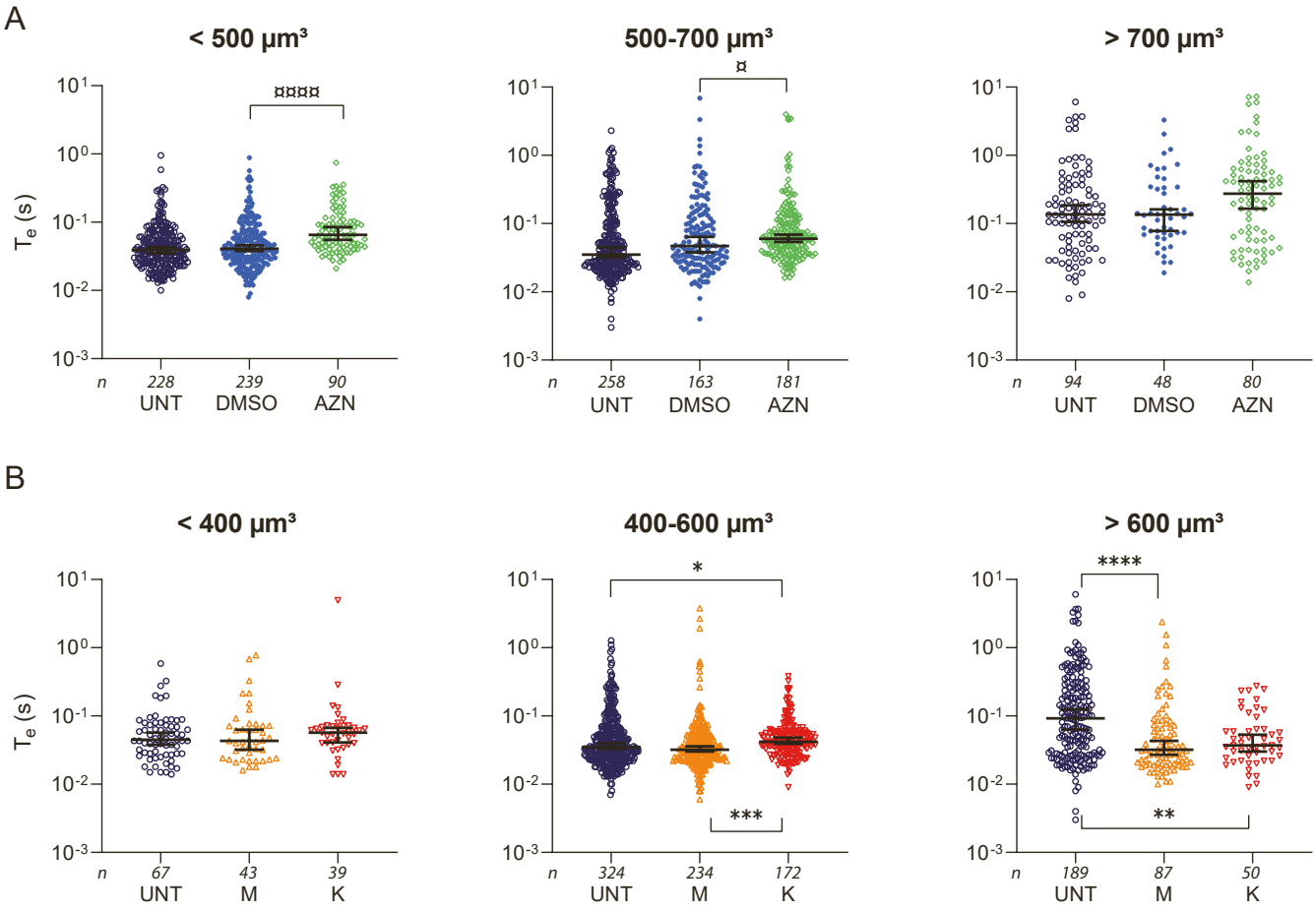

Fig. S9. Entry time of isolated nuclei in constrictions sorted by nucleus volume. Related to Figure 4. Dotplot representations of entry times T_e sorted into three size populations that were defined based on the median volumes of nuclei from AZN cells (≈600 μm^3, B) and from FPLD2 M/K cells (≈500 μm^3, C). Significant differences: AZN *vs* DMSO cells, ¤; FPLD2 *vs* UNT cells, *. Number of experiments: N $\geq$ 4; number of analyzed nuclei: *n*.

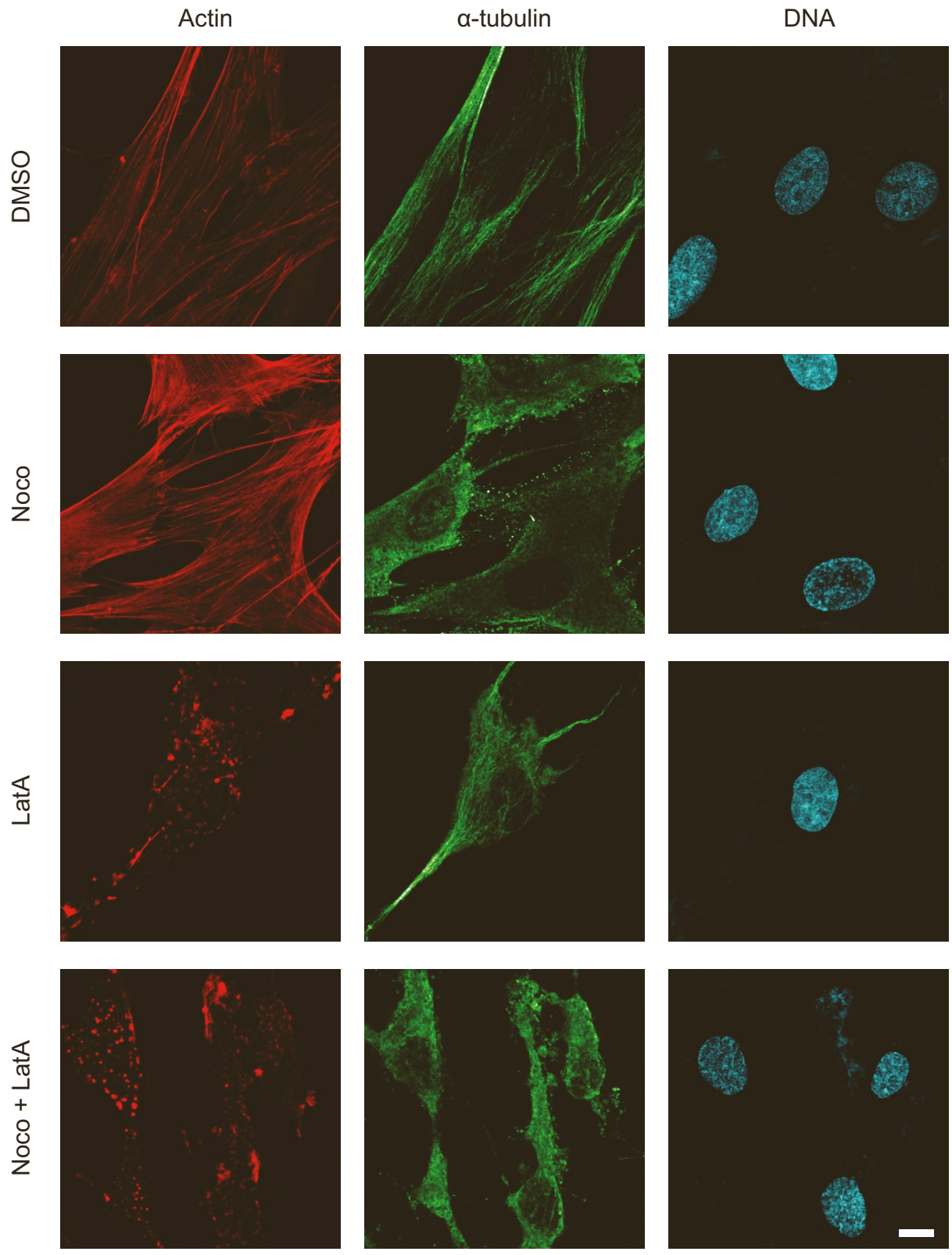

Fig. S10. Actin and microtubule network depolymerization upon cytoskeletal drug treaments. Related to Figure 5. Maximal intensity projection from confocal z-stacks of F-actin (red), α-tubulin (green) and DNA (blue). Adhered UNT cells were incubated with DMSO, or treated with nocodazole (Noco), latrunculine A (LatA) or both nocodazole and latrunculine A (Noco+Lat A) prior to immunostaining. Scale bar: 10 μm.

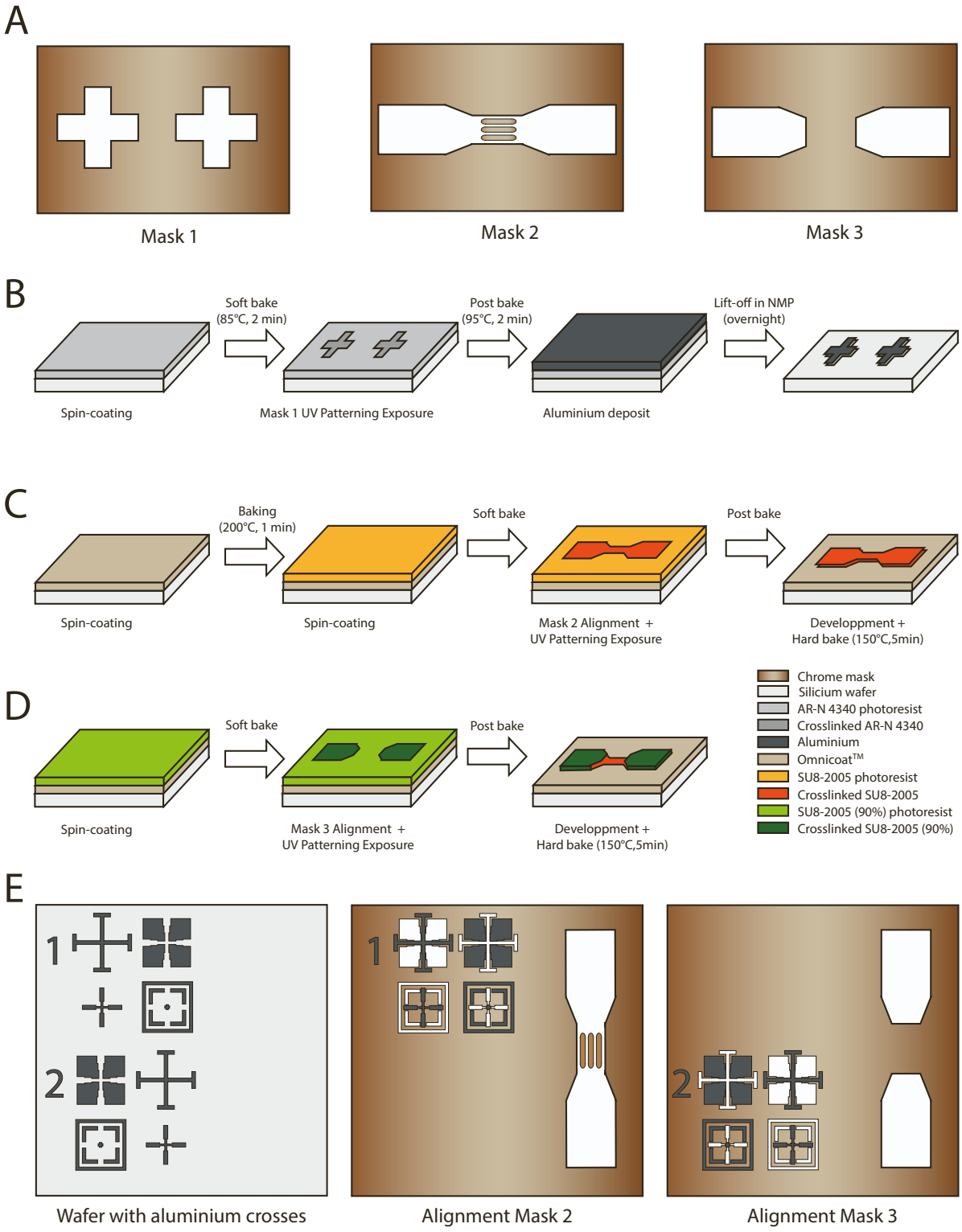

Fig. S11. Workflow of master mold fabrication. Related to STAR Methods. A) Simplified schematics of the three masks used to create the mold: Mask 1, alignment crosses; Mask 2, main channel with micrometer-sized constrictions in the central part; and Mask 3, main channel without constrictions. B-D) Steps to create the two-height master mold. E) Alignment of masks 2 and 3 prior to UV patterning exposure.

UNT				
	DMSO	N	L	NL
T_e (s)	0.48 [0.34-0.60]	0.26 [0.21-0.33]	0.22 [0.18-0.31]	0.15 [0.11-0.18]
η_1 (Pa.s)	26 [22-29]	29 [24-32]	9 [7-11]	10 [8-12]
E (kPa)	5.7 [5.1-6.1]	6.2 [5.6-6.6]	4.5 [4.2-4.9]	4.5 [4.0-5.0]
η_2 (Pa.s)	251 [217-318]	287 [242-335]	146 [112-191]	91 [78-116]
AZN				
	DMSO	N	L	NL
T_e (s)	1.75 [1.33-2.12]	0.95 [0.75-1.20]	0.49 [0.42-0.66]	0.43 [0.36-0.55]
η_1 (Pa.s)	25 [23-28]	34 [28-39]	10 [8-11]	13 [6-16]
E (kPa)	4.0 [3.9-4.3]	4.7 [4.4-5.0]	4.1 [3.8-4.3]	3.9 [3.6-4.3]
η_2 (Pa.s)	700 [582-844]	416 [333-506]	244 [190-302]	181 [138-227]
K				
	DMSO	N	L	NL
T_e (s)	1.26 [0.96-1.49]	0.56 [0.42-0.76]	0.54 [0.40-0.68]	0.41 [0.29-0.59]
η_1 (Pa.s)	23 [19-27]	23 [19-25]	11 [8-13]	11 [9-14]
E (kPa)	4.1 [3.7-4.5]	4.2 3.8-4.6]	3.8 [3.6-4.4]	3.9 [3.4-4.3]
η_2 (Pa.s)	631 [541-725]	293 [247-343]	219 [171-304]	168 [142-219]

Table S1. Changes in rheological parameters upon actin and microtubule networks disruption in UNT, AZN and K cells (medians [95% CI]). Related to Figure 5. Cytoskeleton drugs: N = nocodazole, L = latrunculine A, NL = nocodazole + latrunculin A. Colors indicate significant differences between N/L/NL and DMSO conditions: ns * ** *** ****.